Article

Not peer-reviewed version

Canonical Pathways Rewiring in Alzheimer's Disease

Alejandro Pinta-Castro , Gabriela Michel-Ureña , Alejandra Paulina Pérez-González , Guillermo De Anda-Jáuregui * , Enrique Hernández-Lemus *

Posted Date: 17 April 2026

doi: 10.20944/preprints202604.1194.v1

Keywords: canonical pathways; alzheimer's disease; co-expression networks; GABAergic; glutamatergic; neurexins & neuroligins; SNARE; synaptogenesis

Article

Canonical Pathways Rewiring in Alzheimer's Disease

Alejandro Pinta-Castro [1], Gabriela Michel-Ureña [1], Alejandra Paulina Pérez-González [2,3], Guillermo De Anda-Jáuregui [2,3] and Enrique Hernández-Lemus [2,*]

[1] Facultad Mexicana de Medicina, Universidad La Salle, México City, México
[2] División de Genómica Computacional, Instituto Nacional de Medicina Genómica, México City, México
[3] Programa de Doctorado en Ciencias Biomédicas, Universidad Nacional Autónoma de México, México City, México
[4] Investigadores por México, SECIHTI, Mexico City, Mexico
* Correspondence: gdeanda@inmegen.edu.mx (G.D.A.-J.), ehernandez@inmegen.gob.mx (E.H.-L.)

Abstract

Alzheimer's disease (AD) is a multifactorial neurodegenerative disorder characterized by the simultaneous disruption of interconnected molecular pathways, yet the structural mechanisms underlying this transcriptional disintegration remain poorly characterized. To address this, we constructed condition-specific gene co-expression networks from DLPFC bulk RNA-seq data, using a mutual information framework with Infomap community partitioning. Functional enrichment of network communities via Ingenuity Pathway Analysis (IPA) identified GABAergic signaling, SNARE complex assembly, Synaptogenesis, and Neurexins and Neuroligins interactions as significantly overrepresented pathways. Integration of node degree with condition-specific average expression revealed coordinated topological centralization of key synaptic genes — including NRXN2, LRRTM1, DLGAP3, and SHANK1 — alongside a widespread transcriptional downregulation in GABAergic and Synaptogenesis modules. Shortest path analysis further demonstrated a consistent expansion of intra-pathway distances across all evaluated canonical pathways in AD, quantifying a progressive loss of local communication efficiency. These findings reframe LOAD as an active structural rewiring process, in which the transcriptional network consolidates remaining resources around essential synaptic components as a molecular signature of the pathological state.

Keywords: canonical pathways; alzheimer's disease; co-expression networks; GABAergic; glutamatergic; neurexins & neuroligins; SNARE; synaptogenesis

1. Introduction

Alzheimer's Disease (AD) is the main cause of dementia, accounting for up to 70% of all cases worldwide (Lane et al., 2018; H. Zhang et al., 2020). Late Onset Alzheimer's Disease (LOAD) is typically defined by symptom onset at or after 65 years of age and clinically presents as a progressive disorder characterized by early and prominent episodic memory impairment, which gradually extends to other cognitive domains, including language, visuospatial abilities, and executive function (Rabinovici, 2019). As a result, AD is rapidly becoming one of the most expensive, lethal, and burdensome diseases of this century (Scheltens et al., 2021). The global prevalence of dementia was approximately 50 million people worldwide in 2018 and is projected to triple in 2050 (Scheltens et al., 2021; X. Zhang et al., 2022). Despite significant advances in understanding AD pathogenesis, current treatment strategies generally only ameliorate symptoms, and an effective cure remains elusive (X.-X. Zhang et al., 2021). Since genes do not function in isolation, but rather as part of complex, interconnected modules, deciphering these widespread pathological alterations requires a holistic approach. In this regard, gene co-expression networks provide a systems biology framework for

 doi:10.20944/preprints202604.1194.v1

analyzing the concerted regulation of molecular entities and investigating the dynamic transcriptional landscape in disease (Miller et al., 2008; Thomas & Bonchev, 2010).

This network-based approach allows for the identification of deregulation by characterizing structural changes and reorganizations across three distinct topological scales: macroscopic, microscopic and mesoscopic. At the macroscopic (or global) scale, network analytics evaluate the overall architecture and connectivity patterns of the entire system, such as degree distributions and global cohesion. At the microscopic (or local) scale, this methodology facilitates the detection of individual node properties, such as highly interconnected "hub genes", which play a central role in maintaining system stability and coordinating functional processes (Barabási, 2013). Moreover, it also allows the characterization of mesoscopic alterations (the intermediate structural level), reflected in the reorganization of genes into distinct transcriptional modules or communities (Barabasi & Albert, 1999). Although core biological functions may remain relatively preserved, the specific gene composition within these modules can undergo substantial rearrangement. In this context, functional enrichment analyses of restructured communities and high-betweenness centrality genes have consistently been associated with processes relevant to disease pathology, including synaptic function and synaptic vesicle dynamics (García-Cortés et al., 2021).

Unlike traditional analyses that rely solely on canonical pathways, which are established representations of biological signaling cascades based on prior literature, our data-driven approach captures the actual, condition-specific topological architecture of the transcriptome. By performing co-expression network analysis and integrating it with canonical pathway enrichment, we map these functional co-expression arrangements for each phenotype onto established biological knowledge. This combined strategy aims to interpret the dynamic rewiring of the brain, providing insights into the key molecular networks underlying LOAD pathogenesis. Therefore, the primary problem this study seeks to address is the incomplete understanding of how the brain's transcriptional architecture structurally and functionally rewires in response to the disease, particularly within highly vulnerable regions like the Dorsolateral Prefrontal Cortex (DLPFC).

2. Results

Transcriptional changes in the DLPFC of AD subjects compared to neurologically healthy controls based on average expression analysis identified transcriptional dysregulation across the cortex, characterized predominantly by the downregulation of genes encoding key synaptic and metabolic components. Transcriptional suppression (FDR <0.05) was observed in fundamental transport and vesicular machinery. For instance, the vesicle fusion regulator STXBP1 was significantly downregulated (Log2FoldChange [L2FC] = -0.190; FDR = 0.0037). Similar significant expression deficits were detected for STX1B (L2FC = -0.182; FDR = 0.0075), SYT3 (L2FC= -0.231; FDR = 0.017), and the cell adhesion molecule LRRTM1 (L2FC = -0.246; FDR = 0.0028). Certain central regulatory kinases, such as CDK5 (L2FC = -0.168; FDRj = 0.018), also exhibited marked downregulation in the AD cohort.

2.1. Network Inference and Modular Organization

The AD network exhibited a higher modularity strength (Q = 0.28) compared to the control network (Q = 0.20), indicating a more segregated community structure within the pathological state. The control graph was partitioned into 71 functional communities, whereas the AD graph was partitioned into 68 communities.

The reorganization of gene communities was quantitatively assessed by comparing the modular partitions of the AD and control networks. A Normalized Mutual Information (NMI) score of 0.4479 indicated a rearrangement of gene memberships across modules. Furthermore, the Jaccard similarity index was employed to evaluate the persistence of specific structural communities. The global edge similarity between the networks was approximately 68.39%. Module level comparisons revealed a spectrum of conservation; while certain communities maintained high structural fidelity (e.g., Community 1 exhibited a Jaccard index of 0.88), others displayed significant divergence (e.g., AD

Preprints.org (www.preprints.org) | NOT PEER-REVIEWED | Posted: 17 April 2026 doi:10.20944/preprints202604.1194.v1

community 4 relative to Control community 4 yielded a Jaccard index of 0.58, and AD community 5 mapped to control community 6 with an index of 0.51) (See Figure 1).

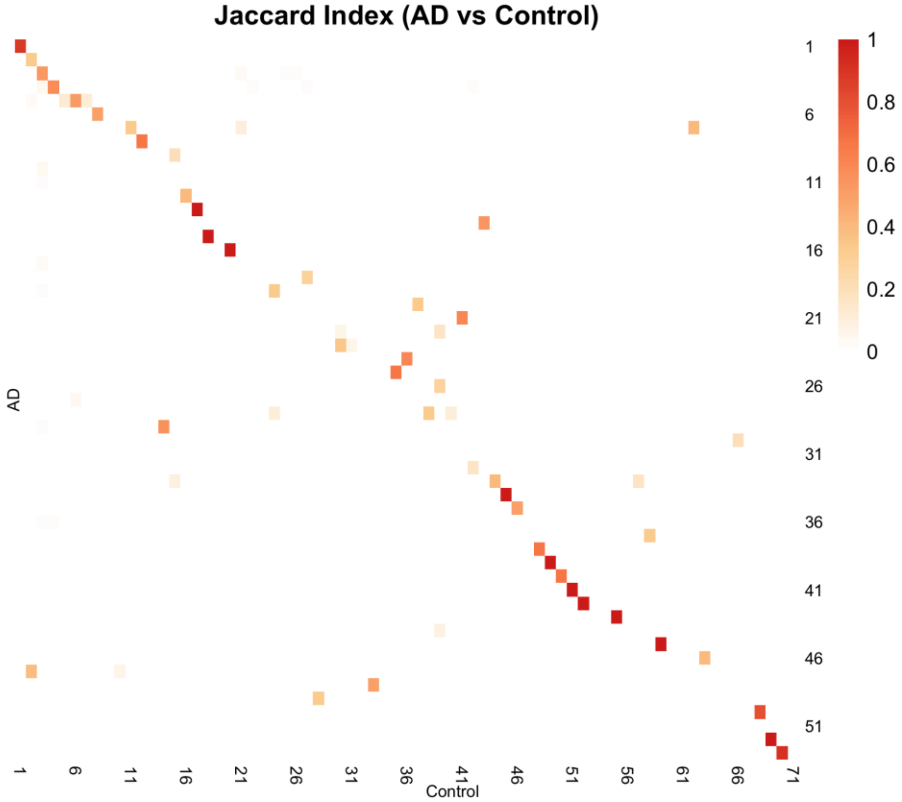

Figure 1. Jaccard index heatmap comparing gene membership similarity between communities in AD and Control networks. Each cell represents the Jaccard Similarity between a pair of communities. The Y-axis shows the AD's communities, while the X-axis represents the Control's communities.

2.2. Pathway Enrichment

Following community partitioning, the structural communities were submitted to IPA for functional characterization. IPA performed an overrepresentation analysis to identify biological functions disproportionately clustered within specific communities. Based on this approach, pathways associated with synaptic structure and function were identified as significantly overrepresented in the AD network communities. Specifically, "synapse organization" (GO:0050808) emerged as highly significant (FDR = 0.0046), driven by the coordinated mapping of genes including NRXN2, LRRTM1, DLGAP3, and SHANK1. Similarly, "synapse assembly" (GO:0007416) was identified as significantly overrepresented (FDR= 0.0074). These pathways were subsequently selected for detailed downstream evaluation based on their statistical significance and biological relevance to AD pathophysiology.

2.3. Network Repositioning Across Median Defined Quadrants

The relationship between transcriptional magnitude and network connectivity was evaluated by mapping genes onto a two-dimensional expression–degree space. Quadrants were defined using the median expression and median degree values across the pathway-specific gene set as threshold boundaries (dashed lines). The upper-right quadrant (Quadrant I) comprises genes with both above-median average expression and above-median connectivity degree, representing highly expressed and highly interconnected nodes. The upper-left quadrant (Quadrant II) included genes with above-median expression but below-median connectivity. The lower-right quadrant (Quadrant IV) corresponded to genes with above-median connectivity but below-median expression, while the lower-left quadrant (Quadrant III) contained genes with both below-median expression and low

 doi:10.20944/preprints202604.1194.v1

connectivity. This framework enabled systematic characterization of coordinated transcriptional and topological shifts between control and AD network.

2.2.1. GABAergic Pathway

Within the GABAergic pathway, GABRB2 and GABRA1 underwent quadrant redistribution from Quadrant II (high expression, low connectivity) to Quadrant I (high expression, high connectivity), driven by a marked increase in interconnectivity. In contrast, GNG3 shifted from Quadrant II to Quadrant III, reflecting a reduction in average expression and relative connectivity, resulting in its repositioning within the lower-expression, lower-connectivity space (see Figure 2).

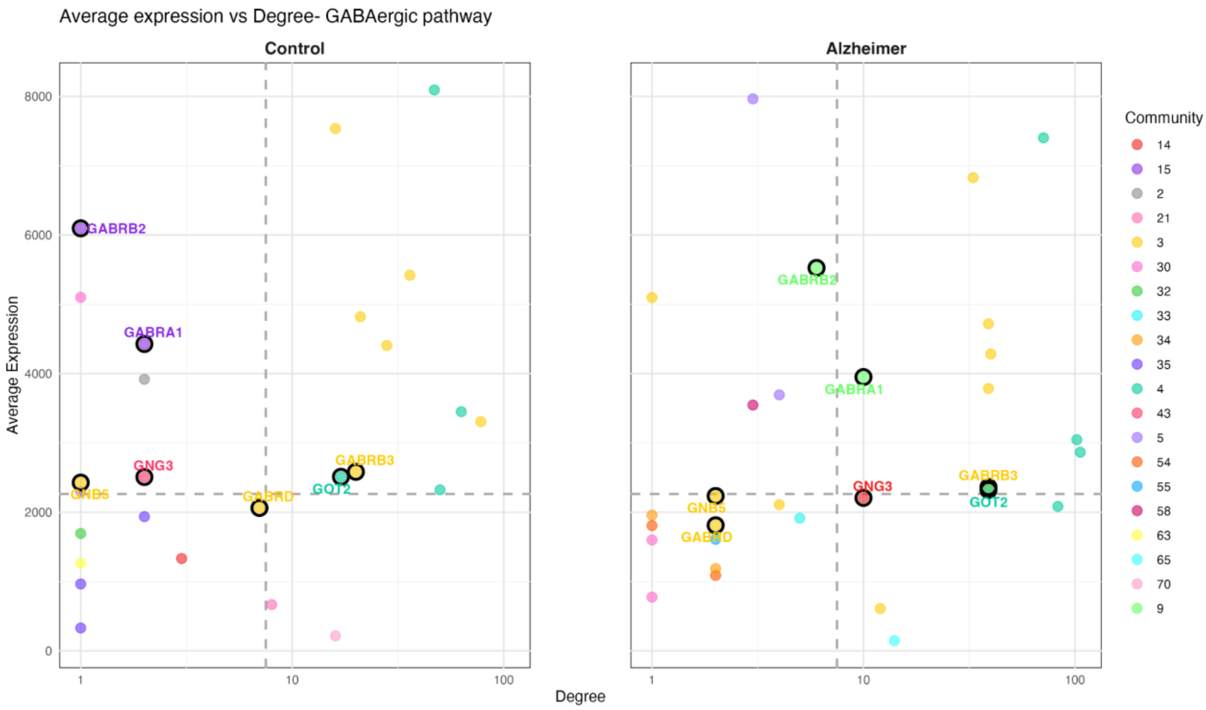

Figure 2. Average expression versus degree of interconnectivity in the GABAergic pathway.

2.2.2. Neurexins and Neuroligins Pathway

Within the Neurexins and Neuroligins pathway, the presynaptic organizer NRXN2 underwent quadrant redistribution from Quadrant II to Quadrant I, driven by an increase in its interconnectivity within the disease network. In contrast, the postsynaptic receptor GRM5 shifted from Quadrant III to Quadrant IV, reflecting a gain in topological centrality despite its average expression remaining below the median threshold (See Figure 3).

Preprints.org (www.preprints.org) | NOT PEER-REVIEWED | Posted: 17 April 2026 doi:10.20944/preprints202604.1194.v1

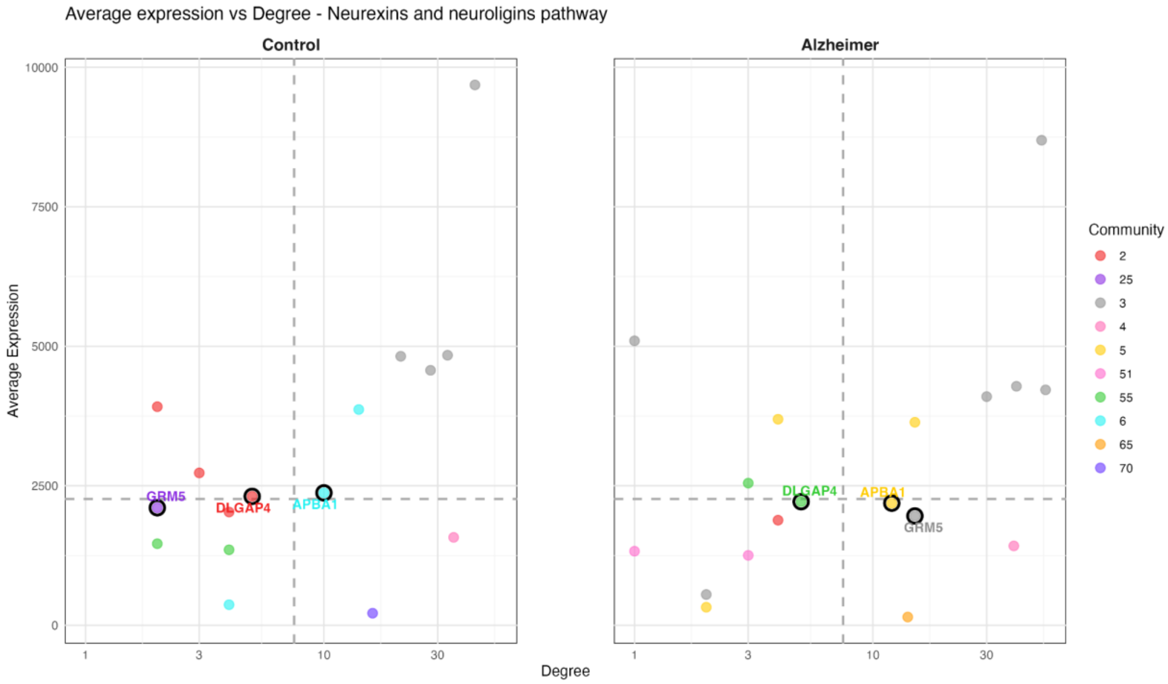

Figure 3. Average expression versus degree of interconnectivity in the Neurexins and Neuroligins pathway.

2.2.3. SNARE Pathway

Within the SNARE pathway, vesicular transport components such as RAB6A and STX1B underwent quadrant redistribution from Quadrant II to Quadrant I, driven by an increase in their interconnectivity. In contrast, the calcium sensing synaptotagmin SYT16 shifted into Quadrant IV, reflecting a gain in connectivity, but with a more than doubling increase in degree, resulting in its repositioning into the higher connectivity space despite lower average expression (See Figure 4).

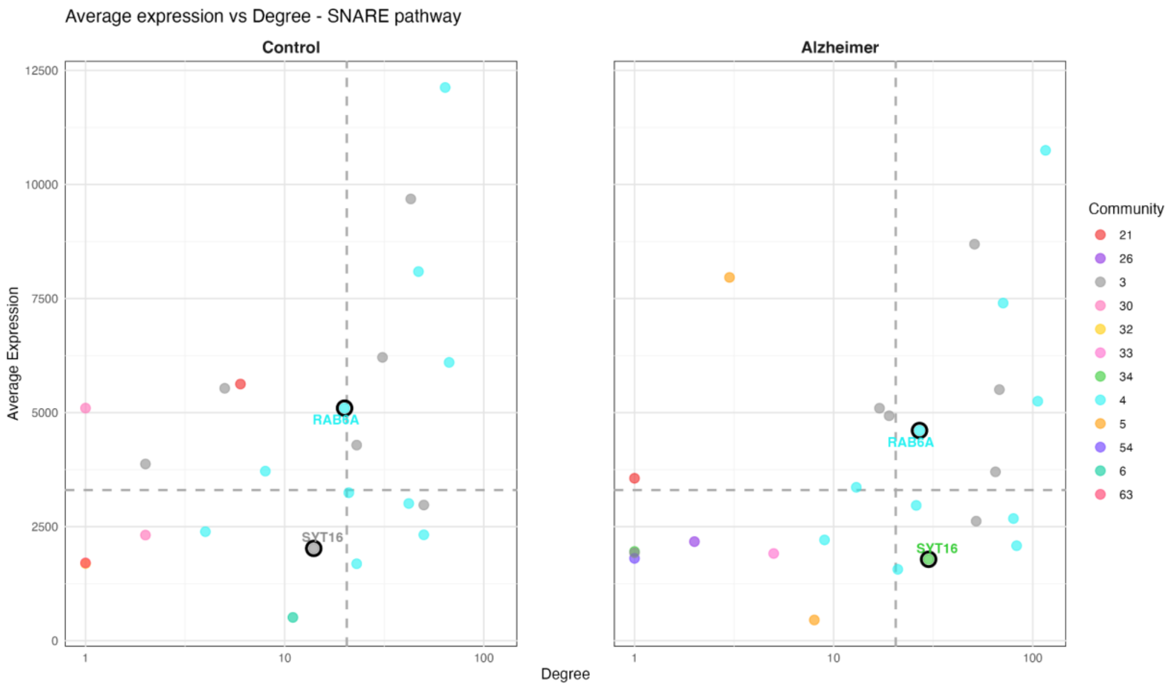

Figure 4. Average expression versus degree of interconnectivity in the SNARE pathway.

2.2.4. Synaptogenesis Pathway

In the synaptogenesis pathway, multiple genes (SYN2, STX1B, WASF1, AP2A1 and SNCA) exhibit a shift from Quadrant II to Quadrant I, showing an increase in interconnectivity and expression. GRM5 shifted from Quadrant IV to Quadrant III, increasing the degree of interconnectivity but remaining constant with its below average expression. SYT3 expressed a discrete shift from Quadrant III towards the margins of Quadrant IV, showing a similar average expression with a decrease of interconnectivity (See Figure 5).

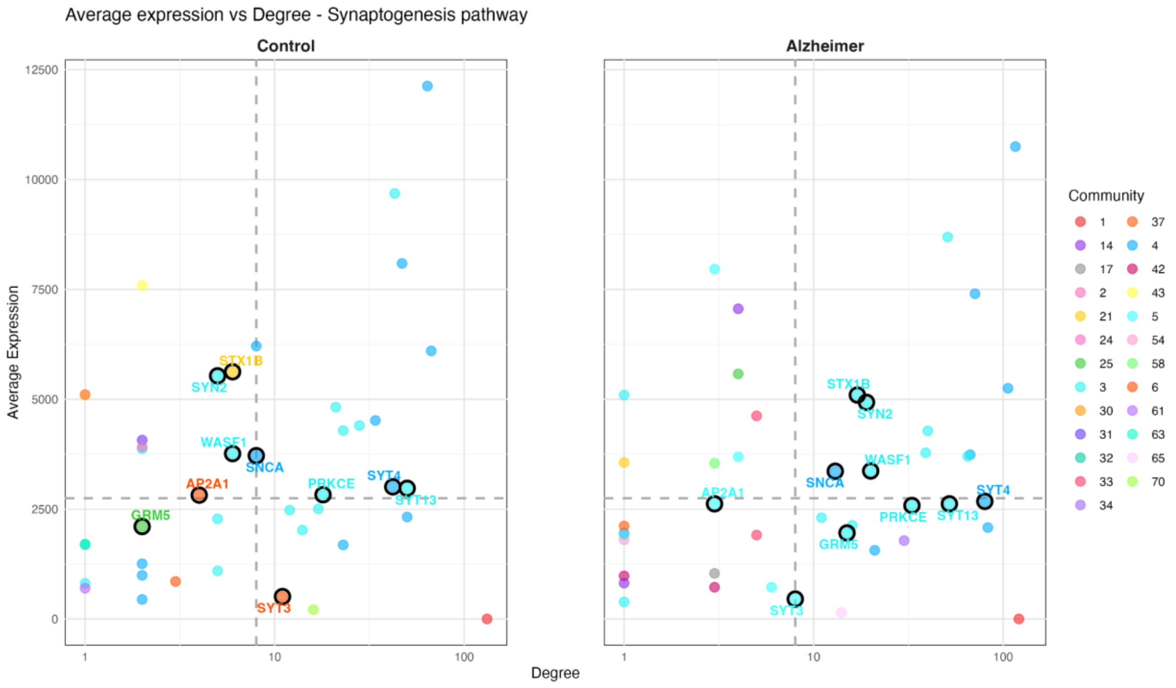

Figure 5. Average expression versus degree of interconnectivity in the synaptogenesis pathway.

2.2.5. Condition Specific Enrichment Patterns

Notably, certain pathways displayed condition specific enrichment patterns. The GABA receptor pathway was significantly enriched only in the control network, whereas the Glutamatergic pathway was exclusively enriched in the AD network. This asymmetrical enrichment highlights differences in pathway representation between conditions.

2.3. Shortest Path Distances in Modules

To evaluate the local communication efficiency and structural integrity of the highly affected modules, shortest path distances were computed between gene nodes within the specific canonical pathways already described. Across all evaluated pathways, the AD network exhibited a distinct increase in mean shortest distances compared to the control network, reflecting a loosening of topological coupling. The expansion of these path lengths, alongside the emergence of fully disconnected gene pairs in the pathological state, quantitatively demonstrates that the transcriptional rewiring in LOAD yields a less communicative architecture.

The loss of routing efficiency was most pronounced within the Synaptogenesis and SNARE pathways. In the control network, the synaptogenesis module displayed a highly coupled structure with a mean shortest distance of 1.55; however, this distance expanded significantly to 2.51 in the AD network. Similarly, the SNARE pathway experienced a substantial topological expansion, with its mean internal distance increasing from 1.83 in control to 2.56 in the AD group. A parallel structural loosening was observed in the primary neurotransmitter networks. The GABAergic signaling pathway exhibited an increase in mean shortest path distance from 1.87 in the control group to 2.09 in the AD group. Finally, the Neurexins and Neuroligins network, which maintained the tightest topological coupling overall, also suffered a loss of efficiency, increasing the adjacent mean distance of 1 in the control network to 1.50 in the AD sample (See Figures 6–9).

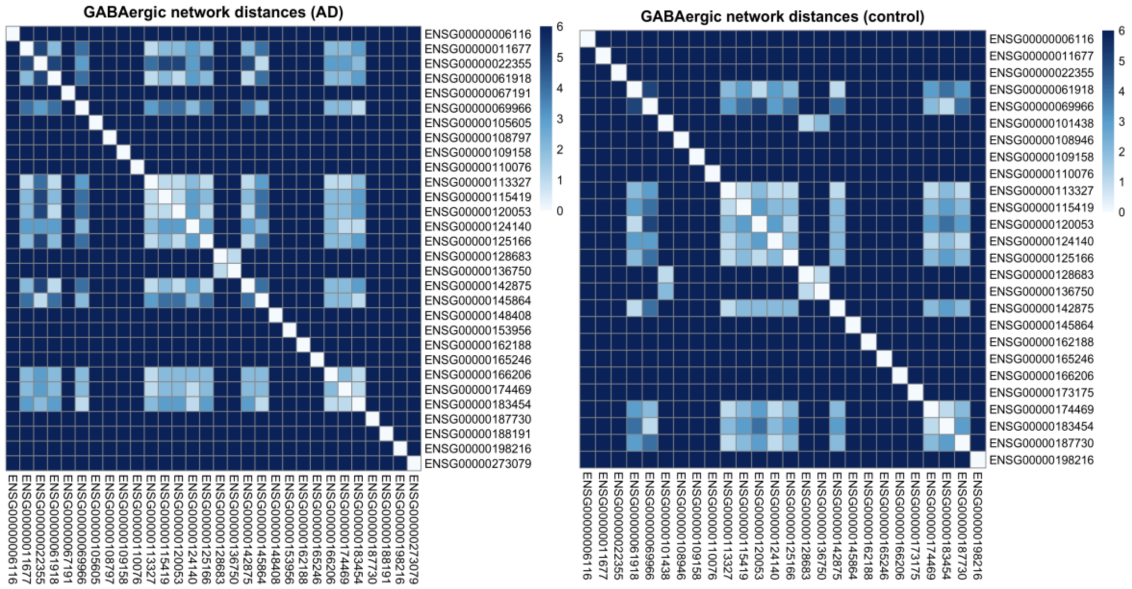

Figure 6. Heatmaps of shortest path distances in the GABAergic network comparing AD and control samples.

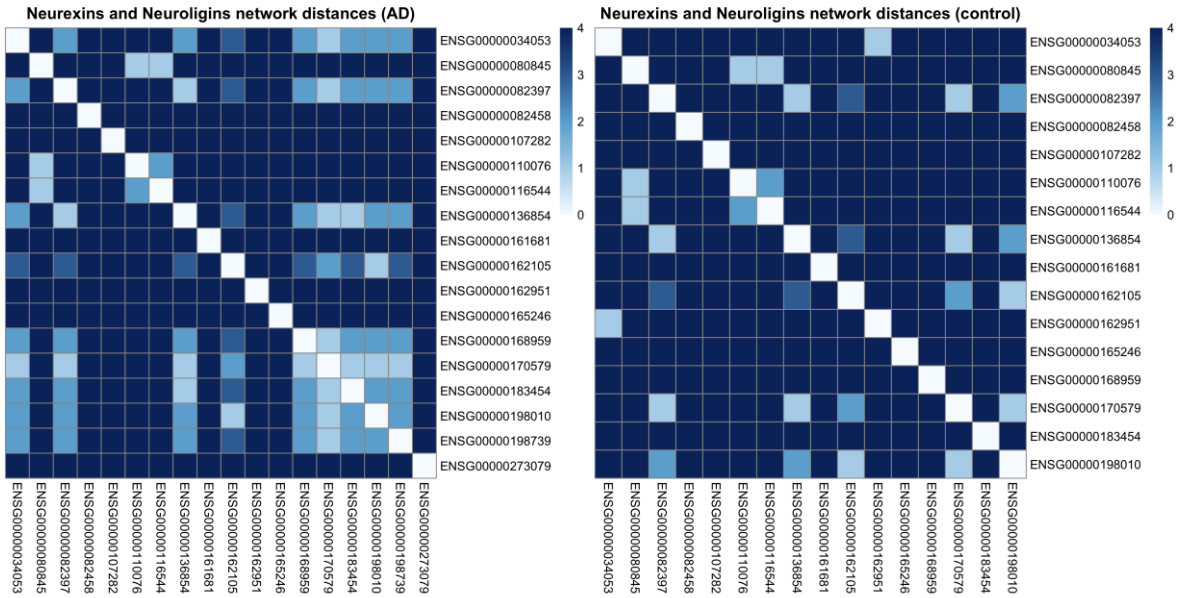

Figure 7. Heatmaps of shortest path distances in the Neurexins and Neuroligins network comparing AD and control samples.

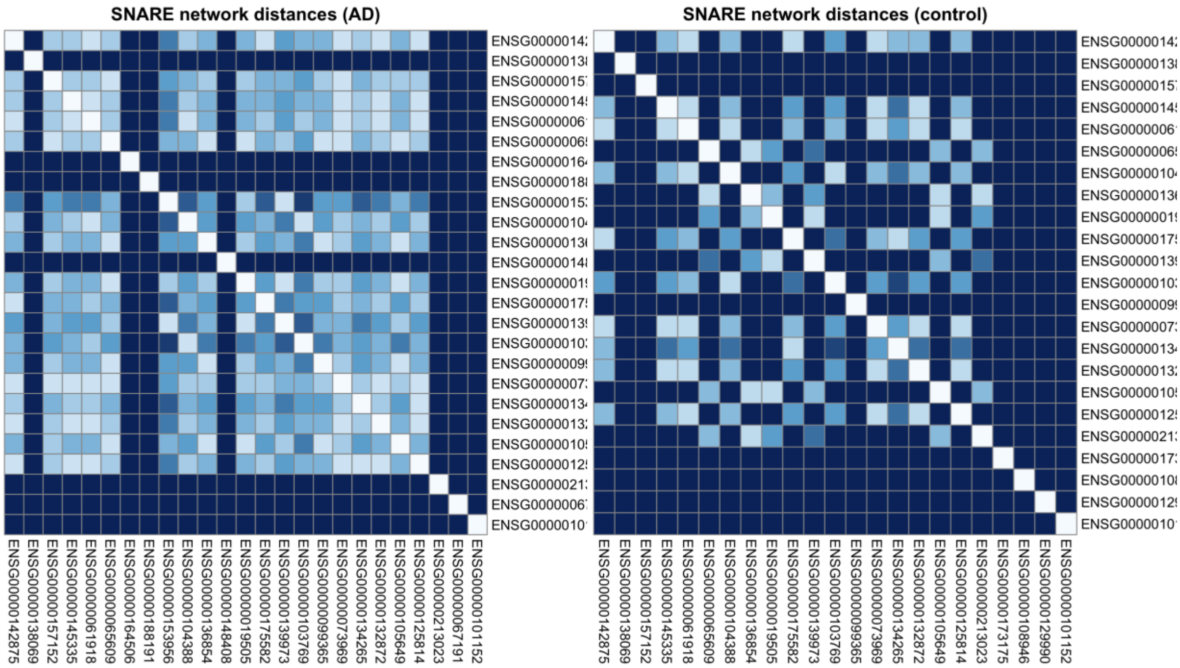

Figure 8. Heatmaps of shortest path distances in the SNARE network comparing AD and control samples.

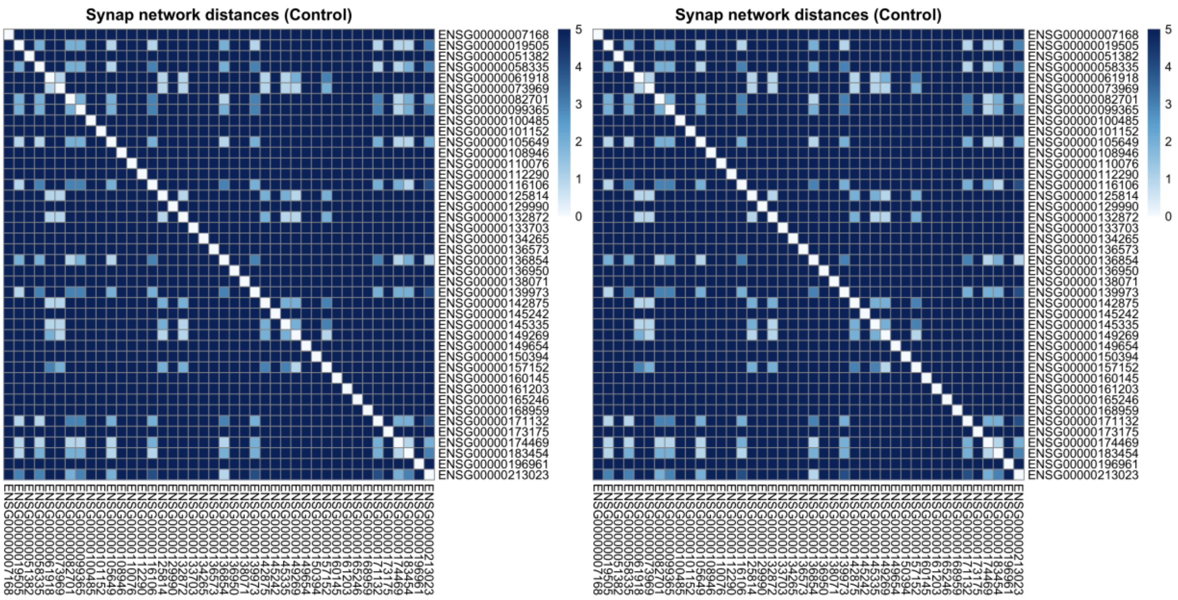

Figure 9. Heatmaps of shortest path distances in the Synaptogenesis network comparing AD and control samples.

3. Discussion

3.1. Confirming the Pathological Baseline

Following our functional analysis, synaptic-related pathways, specifically GABAergic signaling, glutamatergic signaling, SNARE complex, Neurexins and Neuroligins interactions, and Synaptogenesis, emerged as significantly overrepresented. Biologically, the coordination of these genes is essential for establising and maintaining trans-synaptic connections; presynaptic organizaers like NRXN2 bind across the synaptic cleft to postsynaptic organizers such as LRRTM1 to drive bidirectional synaptogenic signals. This trans-synaptic bridge subsequently relies on intracellular postsynaptic scaffolding proteins, including DLGPA3 and SHANK1, to assemble the postsynaptic

Preprints.org (www.preprints.org) | NOT PEER-REVIEWED | Posted: 17 April 2026 doi:10.20944/preprints202604.1194.v1

density, anchor neurotransmitter receptors, and ensure structural integrity for synaptic transmission (Lee et al., 2020) . However, Our analysis revealed a prevalent transcriptional downregulation across these primary synaptic modules. This widespread deterioration aligns with established literature identifying synaptic loss and dysfunction as early, major correlates of cognitive decline in AD. Specifically, the expression deficits observed in the GABAergic and glutamatergic modules confirm the recognized excitatory/inhibitory imbalance that severe suppression of neurotransmitter synthesis confirms the validity and sensitivity of our bulk RNA-seq network approach in capturing the core pathological hallmarks of LOAD (Yin et al., 2021)

3.2. Quantifying the Suspected Network Collapse and Fragmentation

While the recent theories have proposed that AD pathology is driven by an imbalance in cellular communication leading to a “homeostasis network collapse”, out methodology provides concrete quantitative evidence of this structural fragmentation. We demonstrated that the AD network undergoes a profound mesoscopic reorganization characterized by increased modular segregation (modularity strenght $Q = 0.28$ vs $Q = 0.20$) and substantial rearrangement of gene membership (NMI = 0.4479). Biologically, this higher modularity score means that interactions between gene co-expression modules become more isolated from one another under disease conditoins. This structural fragmentation is highly important becasuse it ledas to reduced cross-talk between different functional communities. Reflecting a disrupted regulatory coordination and a loss of efficient flow across the transcriptomic program, this ultimately points to a fundamental breakdown in cellular communication during AD progression (Melo et al., 2024) A key example of this structural loosening is GABRD, which encodes the delta subunit of the GABA-A receptor. GABRD shifted from Quadrant IV to Quadrant III, demonstrating a marked loss of network connectivity. Since this subunit plays a critical role in providing a persistent, low-level inhibitory conductance that stabilizes neuronal excitability, its reduced connectivity quantitatively proves how the loss of this sustained inhibitory “brake” may contribute to the suspected neuronal hyperexcitability observed in AD.

3.3. Evidence of Targeted Adaptation and Topological Centralization

The overall contribution of this study is the discovery of topological centralization via quadrant redistribution. We found that despite the systemic loss of network efficiency, surviving essential functional units, such as GABRA1 and GABRA2, along with transport components like STX1B and SNCA, actively migrate from lower connectivity states (Quadrant II) into highly expressed, highly connected positions (Quadrant I). This suggests a powerful, previously uncharacterized compensatory rewiring mechanism in which the AD network consolidates its remaining resources around specific genes to sustain basic synaptic transmission. It is important to note that we interpret these findings strictly as disease-associated adaptations; the present analysis does not claim that this topological rewiring acts as the primary causal factor driving disease progression, but rather a molecular signature of pathological state. Because this is a newly identified transcriptomic adaptation, future experimental validation will be necessary to contextualize how effectively these topological shifts translate to functional protein-level compensation.

3.4. Diverging from Traditional Degradation Models

Traditional differential expression analyses often portray AD as a uniform, passive degradation of synaptic cascades. Our integration of topology and expression contradicts the assumption that severe transcriptional downregulation equates to a uniform loss of function. By applying condition-specific mean expression values with node degree, we observed that several genes actually gained massive topological influence in the disease state despite reduced or below median expression levels. This discrepancy from prior literature arises because traditionañ analyses rely on static, historically established signaling maps; in contrast, our data-driven co-expression framework captures the dynamic reality of the disease. It shows how the network architecture is actively restructured to

Preprints.org (www.preprints.org) | NOT PEER-REVIEWED | Posted: 17 April 2026 doi:10.20944/preprints202604.1194.v1

preserve essential connectivity, forcing specific remaining components into critical information processing roles to survive the pathological stressor.

3.5. Limitations

Despite the robust methodological approach, several limitations must be transparently acknowledged. First, the cross-sectional design of the ROSMAP RNA-seq data restricts the ability to infer temporal trajectories or sequential rewiring events during the chronological progression of LOAD. Second, the use of bulk RNA-seq data introduces cell-type heterogeneity, meaning that the observed network dynamics represent an aggregate signal of neurons, microglia, and astrocytes, potentially masking distinct, cell-type-specific co-expression shifts (Gutiérrez Cruz et al., 2025). Third, the local structural characterization utilized a pathway-focused shortest path approach based on standardized ring structures constructed via igraph; while informative for local efficiency, this method isolates pathways from the broader global interactome, potentially obscuring wider inter-pathway distances. Furthermore, the targeted evaluation of synaptic pathways was a post-hoc selection; although justified by statistical overrepresentation, this limits unbiased functional discovery outside of those specific neurobiological domains. Lastly, our functional interpretations rely heavily on curated knowledge bases (such as IPA), which are inherently constrained by the current limits of scientific literature and may be subject to annotation bias.

4. Materials and Methods

The methodology used in this study focused on analyzing gene co-expression networks to characterize the transcriptional structure and organization of LOAD in the DLPFC. The workflow was divided into the following stages: data acquisition, classification and quality control, inference of gene co-expression networks, and functional enrichment analysis using Ingenuity Pathway Analysis (IPA) (Krämer et al., 2014) (See Figure 10).

 doi:10.20944/preprints202604.1194.v1

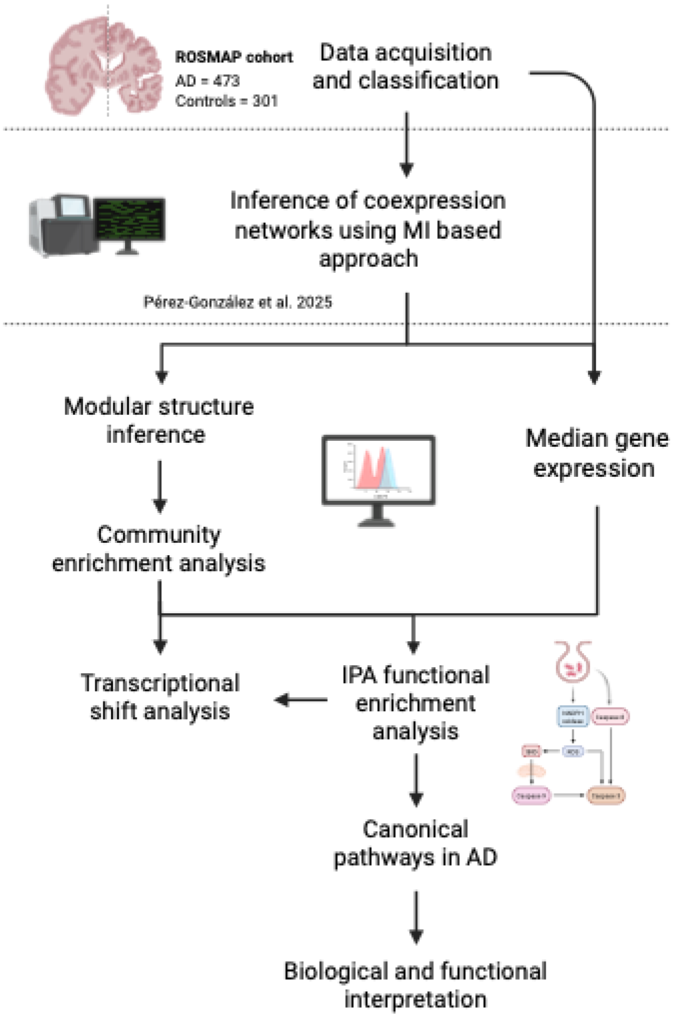

Figure 10. Workflow for Canonical Pathway identification via Network Analysis in Alzheimer's Disease.

Building upon previous systems level findings, this study serves as a direct continuation of the network based characterization of LOAD established by (Pérez-González et al., 2025). Accordingly, the conditions specific gene co-expression networks analyzed herein were obtained from the foundational framework. Briefly, the networks were constructed using DLPFC bulk RNA-seq data from the ROSMAP cohort (473 AD and 301 control subjects) (De Jager et al., 2018). Raw counts were filtered (≥1 CPM), batch corrected with ARSyNSeq (Nueda et al., 2011), and normalized using the Trimmed-Mean-of-M-values (TMM) method. The resulting expression matrices were stratified by NIA-Reagan diagnosis based on metadata to create separate AD and control datasets. Average expression and standard deviation values, corresponding to arithmetic summaries of normalized counts, were computed separately for each biological condition.

For each group, mutual information (MI) between gene expression was calculated using the Infotheo R package (Meyer et al., 2008). To retain only the strongest dependencies, a heuristic cut at the 99.99 percentile of MI values was applied. This specific threshold was selected after evaluating network metrics across multiple percentiles because it optimally filters out noise and weaker, less meaningful associations while retaining a manageable number of nodes and edges, thus preserving the largest connected components and essential topological features. By restricting the network to these highest MI values, we ensure that only the interactions with the most robust dependencies are included, producing undirected networks with identical numbers of edges for fair comparison.

 doi:10.20944/preprints202604.1194.v1

Network topology was examined with the igraph package (Csardi & Nepusz, 2006) focusing on degree and betweenness centrality to identify hub and high betweenness genes. Degree values represent the number of edges connected to each gene node within the MI based co-expression network, and community labels corresponding to modules identified via Infomap partitioning.

Community structure was inferred with the Infomap algorithm (Smiljanić et al., 2026), yielding 68 AD modules and 71 control modules. Community similarity between the independently inferred AD and control MI based co-expression networks was quantified using the Jaccard index. Specifically, for each community identified in the control network, Jaccard similarity was computed based on gene membership overlap. Functional enrichment of modules and central nodes was performed using clusterProfiler on GO Biological Process terms (p-value < 0.05, False Discovery Rate [FDR] < 0.05).

Functional enrichment and pathway analysis were performed using Ingenuity Pathway Analysis (IPA) Qiagen. Two input tables were independently submitted to this platform, each corresponding to one biological condition (control and AD). These tables contained each gene metric derived from the network analyses, including: average expression standard deviation, node degree within the inferred co-expression network and community assignment as determined by network partitioning.

Upon submission, IPA mapped gene identifiers to its proprietary knowledge base and performed enrichment analyses using its curated molecular interaction libraries. These libraries integrate experimentally validated and literature derived relationships encompassing canonical pathways, upstream regulators, molecular interactions, disease associations, and functional annotations. Enrichment statistics were computed internally by IPA using right-tailed Fisher's exact tests to evaluate overrepresentation of input genes within curated gene sets. To ensure robust statistical significance and correct for multiple comparisons, a FDR) threshold of < 0.05 was applied. This threshold thereby complemented the user provided quantitative and network derived metrics with knowledge driven biological context, enabling integration of transcriptomics, network topology, and curated pathways knowledge to generate a multidimensional functional interpretation of specific network structure.

The structural reorganization of synaptic and metabolic pathways between AD and control conditions was evaluated by integrating expression magnitude with community overlap and graph derived distanced metrics.

Shortest path distances were computed for pathway-specific gene sets corresponding to the canonical pathways in Alzheimer and control samples using the original co-expression networks. Gene identifiers from the selected pathway were first filtered, cleaned, and intersected with the node sets of each condition-specific graph to retain only genes present in the respective networks. For each condition, an induced subgraph was then constructed from the full network, preserving the original topology among the selected genes rather than imposing an artificial structure. Pairwise shortest path distances between all nodes within each subgraph were calculated using the distances() function from the igraph package, generating symmetric distance matrices representing the minimum number of edges separating each pair of genes. Infinite matrices, corresponding to disconnected node pairs, were excluded from summary statistics. Mean shortest path distances were computed for each condition as a global measure of network proximity within the pathway. The resulting distance matrices were visualized as clustered heatmaps using hierarchical clustering and exported for analyses.

In conclusion, our multidimensional network analysis reveals that LOAD is not merely a disease of isolated transcriptional deficits, but complex, active structural rewiring of the brain's functional architecture. The AD transcriptome shifts from a state of hemostatic integration to one of modular isolation, compelling specific emergent hub genes to shoulder the burden of synaptic communication. Identifying and targetinf these highly centralized, compensatory genes offers a promising new paradigm for therapeutic interventions aimed at stabilizing synaptic function in AD.

Supplementary Materials: The following supporting information can be downloaded at the website of this paper posted on Preprints.org.

Author Contributions: Conceptualization, E.H.L., G.D.J.; methodology, A.P.C., A.P.P.G., and G.D.J.; software: A.P.P.G., and G.D.J.; validation, A.P.C. and G.M.U.; formal analysis, E.H.L., G.D.J.; investigation, A.P.C. and G.M.U; resources, E.H.L. and G.D.J.; data curation, A.P.P.G., A.P.C., G.M.U.; writing—original draft preparation, A.P.C.; writing—review and editing, A.P.C., G.M.U., A.P.P.G., G.D.J. and E.H.L.; visualization, A.P.C., A.P.P.G.,.; supervision, E.H.L. and G.D.J.; project administration, E.H.L. and G.D.J. funding acquisition, E.H.L. and G.D.J. All authors have read and agreed to the published version of the manuscript.

Funding: The author(s) declare financial support was received for the research, authorship, and/or publication of this article. A.P.P.-G. is a doctoral student from Programa de Doctorado en Ciencias Biomédicas (PDCB), Universidad Nacional Autónoma de México (UNAM), and received fellowship 904078 from CONAHCYT (now SECIHTI). Study data were provided by the Rush Alzheimer's Disease Center, Rush University Medical Center, Chicago. Data collection was supported through funding by NIA grants P30AG10161 (ROS), R01AG15819 (ROSMAP; genomics and RNAseq), R01AG17917 (MAP), R01AG30146, R01AG36042 (5hC methylation, ATACseq), RC2AG036547 (H3K9Ac), R01AG36836 (RNAseq), R01AG48015 (monocyte RNAseq) RF1AG57473 (single nucleus RNAseq), U01AG32984 (genomic and whole exome sequencing), U01AG46152 (ROSMAP AMP-AD, targeted proteomics), U01AG46161 (TMT proteomics), U01AG61356 (whole genome sequencing, targeted proteomics, ROSMAP AMP-AD), the Illinois Department of Public Health (ROSMAP), and the Translational Genomics Research Institute (genomic). Additional phenotypic data can be requested at http://www.radc.rush.edu.

Informed Consent Statement: "Informed consent was obtained from all subjects involved in the study."

Data Availability Statement: ROSMAP data can be requested at http://www.radc.rush.edu. All code involved in this work is publicly available at the following link: https://github.com/CSB-IG/ROSMAP_MultiOmics/tree/main/ROSMAP-rnaseq-networks (accessed on 3 March 2025).

Conflicts of Interest: "The authors declare no conflicts of interest. The funders had no role in the design of the study; in the collection, analyses, or interpretation of data; in the writing of the manuscript; or in the decision to publish the results".

References

1. Durinck S, Spellman P, Birney E, Huber W (2009). "Mapping identifiers for the integration of genomic datasets with the R/Bioconductor package biomaRt." Nature Protocols, 4, 1184–1191.
2. Barabási, A.-L. (2013). Network science. Philosophical Transactions of the Royal Society A: Mathematical, Physical and Engineering Sciences, 371(1987), 20120375. https://doi.org/10.1098/rsta.2012.0375
3. Barabasi, A.-L., & Albert, R. (1999). Emergence of scaling in random networks. Science, 286(5439), 509–512. https://doi.org/10.1126/science.286.5439.509
4. García-Cortés, D., Hernández-Lemus, E., & Espinal-Enríquez, J. (2021). Luminal A Breast Cancer Co-expression Network: Structural and Functional Alterations. Frontiers in Genetics, 12, 629475. https://doi.org/10.3389/fgene.2021.629475
5. Gutiérrez Cruz, A. I., de Anda-Jáuregui, G., & Hernández-Lemus, E. (2025). Gene Co-Expression Analysis Reveals Functional Differences Between Early- and Late-Onset Alzheimer's Disease. Current Issues in Molecular Biology, 47(3), 200. https://doi.org/10.3390/cimb47030200
6. Lane, C. A., Hardy, J., & Schott, J. M. (2018). Alzheimer's disease. European Journal of Neurology, 25(1), 59–70. https://doi.org/10.1111/ene.13439

 doi:10.20944/preprints202604.1194.v1

7. Lee, A. K., Khaled, H., Chofflet, N., & Takahashi, H. (2020). Synaptic Organizers in Alzheimer's Disease: A Classification Based on Amyloid-β Sensitivity. Frontiers in Cellular Neuroscience, 14, 281. https://doi.org/10.3389/fncel.2020.00281
8. Melo, D., Pallares, L. F., & Ayroles, J. F. (2024). Reassessing the modularity of gene co-expression networks using the Stochastic Block Model. PLOS Computational Biology, 20(7), e1012300. https://doi.org/10.1371/journal.pcbi.1012300
9. Miller, J. A., Oldham, M. C., & Geschwind, D. H. (2008). A Systems Level Analysis of Transcriptional Changes in Alzheimer's Disease and Normal Aging. The Journal of Neuroscience, 28(6), 1410–1420. https://doi.org/10.1523/JNEUROSCI.4098-07.2008
10. Rabinovici, G. D. (2019). Late-onset Alzheimer Disease. Continuum : Lifelong Learning in Neurology, 25(1), 14–33. https://doi.org/10.1212/CON.0000000000000700
11. Scheltens, P., Strooper, B. D., Kivipelto, M., Holstege, H., Chételat, G., Teunissen, C. E., Cummings, J., & van der Flier, W. M. (2021). Alzheimer's disease. Lancet (London, England), 397(10284), 1577–1590. https://doi.org/10.1016/S0140-6736(20)32205-4
12. Thomas, S., & Bonchev, D. (2010). A survey of current software for network analysis in molecular biology. Human Genomics, 4(5), 353–360. https://doi.org/10.1186/1479-7364-4-5-353
13. Yin, W., Mendoza, L., Monzon-Sandoval, J., Urrutia, A. O., & Gutierrez, H. (2021). Emergence of co-expression in gene regulatory networks. PLOS ONE, 16(4), e0247671. https://doi.org/10.1371/journal.pone.0247671
14. Zhang, H., Chen, W., Tan, Z., Zhang, L., Dong, Z., Cui, W., Zhao, K., Wang, H., Jing, H., Cao, R., Kim, C., Safar, J. G., Xiong, W.-C., & Mei, L. (2020). A Role of Low-Density Lipoprotein Receptor-Related Protein 4 (LRP4) in Astrocytic Aβ Clearance. The Journal of Neuroscience: The Official Journal of the Society for Neuroscience, 40(28), 5347–5361. https://doi.org/10.1523/JNEUROSCI.0250-20.2020
15. Zhang, X., Zou, M., Wu, Y., Jiang, D., Wu, T., Zhao, Y., Wu, D., Cui, J., & Li, G. (2022). Regulation of the Late Onset alzheimer's Disease Associated HLA-DQA1/DRB1 Expression. American Journal of Alzheimer's Disease and Other Dementias, 37, 15333175221085066. https://doi.org/10.1177/15333175221085066
16. Zhang, X.-X., Tian, Y., Wang, Z.-T., Ma, Y.-H., Tan, L., & Yu, J.-T. (2021). The Epidemiology of Alzheimer's Disease Modifiable Risk Factors and Prevention. The Journal of Prevention of Alzheimer's Disease, 8(3), 313–321. https://doi.org/10.14283/jpad.2021.15
17. Author 1, A.B. Title of Thesis. Level of Thesis, Degree-Granting University, Location of University, Date of Completion.
18. Title of Site. Available online: URL (accessed on Day Month Year).